Pergamon

*Int. J. Solids Structures* Vol. 33, No. 18, pp. 2659–2680, 1996

0020 7683/96 $15.00 + .00

0020–7683(95)00169–7

# DYNAMIC BEHAVIOUR OF ELASTIC-PLASTIC FREE-FREE BEAMS SUBJECTED TO IMPULSIVE LOADING

T. X. YU*, J. L. YANG, S. R. REID
Department of Mechanical Engeering, UMIST, P.O. Box 88, Manchester M60 1QD, U.K.

and

C. D. AUSTIN
Aberdeen College, Gallowgate, Aberdeen AB9 1DN, U.K.

(*Received* 28 *June* 1994)

**Abstract**—A dynamic analysis of an elastic-plastic free-free beam subjected to impact by a projectile at the mid-span or to triangularly distributed impulsive loading along the span is presented. Attention is focused on the dynamic behaviour of the beam in the early, transient stage of the response. Details of the interactions between the plastic flexural wave and the elastic flexural wave reflected from the free ends are described, which assist in understanding how the elastic effect modifies the deformation history of a beam and finally leads to a somewhat different configuration from that based on a rigid-perfectly plastic model. The partitioning of the energy in the deformed beam is also examined and a rigid-plastic model with a rotational elastic-plastic spring at the mid-span of the beam is proposed in order to estimate the proportions of elastic energy and plastic dissipation. To verify the theoretical predictions, a group of high-speed photographs obtained experimentally for central impact of a free-free beam is presented and compared with the numerical results on the instantaneous profiles of the beam. Copyright © 1996 Elsevier Science Ltd.

## NOTATION

| | |
|---|---|
| $b$ | width of a beam |
| $E$ | Young's modulus |
| $E_p$ | strain hardening modulus |
| $G$ | one half of impact mass |
| $h$ | depth of beam |
| $I$ | second moment of cross-section of a beam |
| $J$ | rotary inertia of cross-section per unit length of a beam |
| $K_c$ | kinetic energy of rigid-body motion, i.e. the kinetic energy carried by the mass centre of the beam and the projectile |
| $k$ | elastic constant of a rotational spring |
| $L$ | half length of a free-free beam |
| $M$ | bending moment |
| $M^*$ | bending moment when unloading starts |
| $M_e$ | maximum elastic bending moment |
| $M_p$ | fully plastic bending moment |
| $M_s$ | defined in eqn (18) |
| $m$ | mass per unit length of a beam |
| $P(t)$ | concentrated force pulse |
| $p(x, t)$ | distribution load along a beam |
| $Q$ | shear force |
| $R$ | energy ratio, $= W_o/W_e^{max}$ |
| $t$ | time |
| $U$ | displacement of the mid-point of a beam |
| $u$ | non-dimensional displacement, $= U/L$ |
| $V_0$ | initial velocity of impact mass |
| $V_c$ | velocity of the mass centre |
| $W_e$ | elastic deformation energy which is exchangeable with the "local kinetic energy" |
| $W_e^{max}$ | maximum elastic deformation energy that a beam can store |
| $W_o$ | total input energy |
| $W_p$ | plastic dissipation based on elastic-plastic theory |

*Current address: Department of Mechanical Engineering, Hong Kong University of Science and Technology, Hong Kong.

| | |
|---|---|
| $W_p^r$ | plastic dissipation based on rigid-plastic theory |
| $w$ | transverse displacement |
| $x, y$ | dimensional coordinates |
| $x_1, x_2$ | distances from the mid-point |
| $Y$ | yield stress |
| $\beta$ | mass ratio, $= G/mL$ |
| $\kappa$ | curvature |
| $\kappa^*$ | curvature when unloading starts |
| $\kappa_e$ | maximum elastic curvature |
| $\theta$ | rotation angle |
| $\theta_p$ | plastic rotation angle |
| $\Lambda$ | terminal position of a travelling hinge |
| $\lambda$ | $= \Lambda/L$ |
| $\tau$ | non-dimensional time |
| $\dot{(\ )}$ | $\partial(\ )/\partial(t)$ |
| $(\ )'$ | $\partial(\ )/\partial(\tau)$. |

## 1. INTRODUCTION

The dynamic behaviour and failure of free-free beams under intense dynamic loading are of interest when placed in the context of aerospace engineering applications. The intense dynamic loading may be produced by impact from a projectile or detonating an explosive. When such loading acts on a free-free beam, it can undergo gross plastic deformation when the energy input to the structure significantly exceeds the maximum elastic energy that the beam can store. However, for a symmetrically loaded free-free beam, the final translational kinetic energy of its rigid body motion may take up a large portion of the input energy, and, consequently, reduce greatly the energy dissipated in plastic deformation. Energy conservation requires that

$$W_o = K_c + W_e + W_p, \tag{1}$$

where $W_o$ is the total input energy; $K_c$ denotes the kinetic energy of the rigid-body motion, i.e. the kinetic energy carried by the centre of mass of the beam (and the projectile if there is one); $W_e$ denotes the elastic deformation energy which (or a portion of which) is exchangeable with the "local kinetic energy" that accounts for the difference between the sum of kinetic energy of all the individual elements and $K_c$; and $W_p$ denotes the plastic dissipation. It is usually supposed that the dynamic failure (i.e. collapse) of the beam is only caused by the plastic dissipation $W_p$.

The analysis of the dynamic response of structures subjected to intense dynamic loading is greatly simplified by adopting the rigid, perfectly-plastic idealization which neglects the elastic deformation of the material. When the input energy is much larger than the maximum elastic energy a structure can store, the rigid-plastic analysis is found to provide a good estimate of the overall response of the structure, especially of the permanent deformation. The dynamic behaviour of rigid-plastic free-free beams under pulse loading was first studied by Lee and Symonds (1952) who revealed the location of plastic hinges in response to a varying load pulse. Succeeding works, e.g. Symonds (1953), Symonds and Leth (1954) were also based on the rigid-plastic idealization.

More recently, Jones and Wierzbicki (1987) conducted a study of dynamic plastic failure (i.e. collapse) of a free-free beam of uniform or stepped cross-section under a triangularly distributed impulsive load. They concluded that only 25% of the input energy is converted into plastic work for an ideal impulse. The remaining 75% of the input energy results in rigid-body motion. As their theoretical analysis is based on the rigid, perfectly-plastic idealization for the material, the amount of plastic work is overestimated due to the neglect of elastic deformation energy. In spite of this, their result is still a quite good estimation of the energy partitioning in a free-free beam when the impulsive loading has a sufficient intensity that 25% of the input energy (i.e. the work done by the external loads) is much larger than the elastic strain energy capacity of the beam.

Unlike examples such as simply supported and clamped beams, for which all of the input energy is converted only into the elastic deformation energy and plastic dissipation, a free-free beam may display a very different behaviour regarding energy partitioning. After

the kinetic energy of rigid body motion is subtracted from the total input energy, the elastic deformation energy can be much more important than might be expected at first sight, especially when the input energy (i.e. the work done by the external loads) is not far in excess of the maximum elastic capacity of the beam. Therefore, more care needs to be taken when one uses a rigid-plastic model to analyze the dynamic response and plastic collapse of a free-free beam.

Furthermore, elastic effects in this problem may not only be confined to the equation of energy conservation; they may also alter the deformation history of the beam and lead to a distribution of plastic deformation in the deformed beam which is significantly different from that in a rigid, perfectly-plastic beam. Finite element calculations have been reported on the elastic-plastic response of beams subjected to impact. By using the ABAQUS code, Symonds and Fleming (1984) and Reid and Gui (1987) carefully studied the dynamic behaviour of elastic-plastic cantilever beams subjected to tip impact by a projectile and found that in the early transient phase of the response, the interaction between the main plastic bending wave and the elastic bending wave reflected from the clamped end makes the dynamic response of the beam more complex. As a result of this interaction, a high curvature region (or a "kink") is formed in the interior of the beam, which was observed in a previous test (see Hall *et al.* (1971)) but which cannot be predicted by rigid-plastic approaches.

An analysis of the dynamic behaviour of an elastic-plastic free-free beam subjected to impact at mid-span by a projectile (Fig 1(a)) or to triangularly distributed impulsive loading (Fig 1(b)) is presented in this paper, with the help of a numerical solution of the governing equations based on a small deflection formulation. Emphasis is placed on the transient behaviour of the beam after impact and the final partitioning of the plastic dissipation, the elastic deformation energy and the kinetic energy of rigid-body motion for the deformed beam. As an example, a set of numerical results corresponding to a free-free beam whose response was observed experimentally is given and compared with the experimental data on the instantaneous profiles of the beam and the terminal positions of the plastic deformation in the beams.

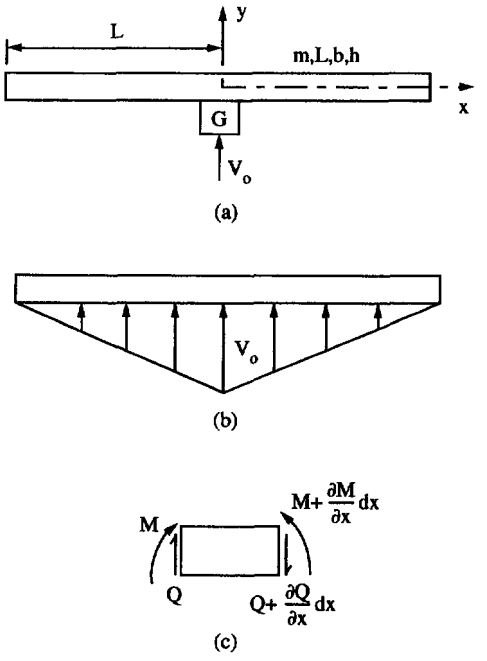


Fig. 1. A free-free beam subjected to dynamic loading: (a) impact at the mid-span by a projectile; (b) triangularly distributed impulsive loading; (c) internal forces acting on an element.

## 2. ELASTIC-PLASTIC ANALYSIS

### 2.1. *Equations of motion*

A typical element of the beam is shown in Fig. 1(c) with the $x$ and $y$ axes being in the axial and transverse directions, respectively. The internal forces acting on the element are the lateral shear force $Q$ and the bending moment $M$. If the external force acting on the element, $p(t, x)$, is in the transverse direction only, and the deflection remains small in comparison with the length of the beam, the equations of motion of the element are

$$\frac{\partial Q}{\partial x} + m\ddot{w} = p(x, t), \tag{2}$$

$$\frac{\partial M}{\partial x} - Q = J\frac{\partial \ddot{w}}{\partial x}, \tag{3}$$

where $w$ is the transverse deflection, $m$ and $J$ are the mass and rotary inertia of the beam per unit length, respectively. Eliminating shear force $Q$ from eqns (2) and (3) gives

$$\frac{\partial^2 M}{\partial x^2} + m\ddot{w} - J\frac{\partial^2 \ddot{w}}{\partial x^2} = p(x, t). \tag{4}$$

It is evident that eqn (4) is applicable to beams with arbitrary material properties, provided their cross-sections remain unchanged during the flexural deformation and the deflections are small. The rotary inertia of a cross-section of the beam is included here in order to model more precisely the propagation of the elastic flexural wave.

### 2.2. *Constitutive relations*

The free-free beam is assumed to have uniform rectangular cross-section and to be made of an elastic-perfectly plastic material. Thus, the constitutive relations between bending moment $M$ and curvature $\kappa$ ( $= \partial w^2/\partial x^2$ in the case of small deflections) can be written in the form of (see Fig. 2):

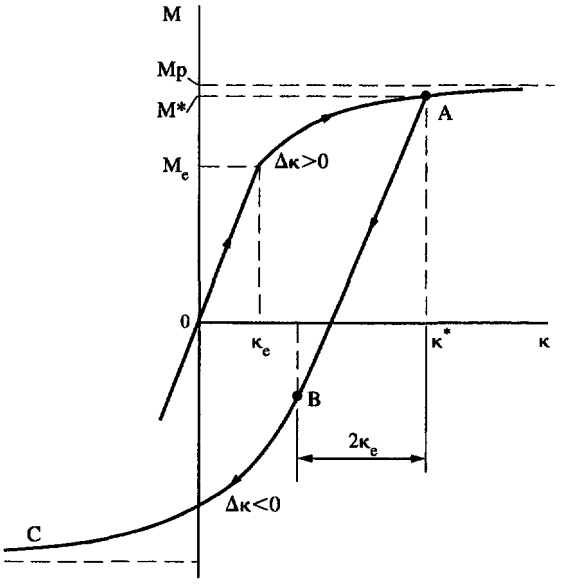


Fig. 2. The bending moment–curvature relationship of a beam made of an elastic, perfectly-plastic material.

$$M = \begin{cases} EI\kappa, & 0 \leqslant \kappa \leqslant \kappa_e; \\ M_e\left[\dfrac{3}{2} - \dfrac{1}{2}\left(\dfrac{\kappa_e}{\kappa}\right)^2\right], & \kappa_e < \kappa, \quad \Delta\kappa > 0, \end{cases} \tag{5a}$$

where $M_e = Ybh^2/6$ is the maximum elastic bending moment for a beam of rectangular cross-section; $\kappa_e = M_e/EI = 2Y/Eh$ is the maximum elastic curvature; $I = bh^3/12$ with $b$ and $h$ being the width and depth of the cross-section; $E$ and $Y$ are the Young's modulus and yield stress of the material, respectively; and $\Delta\kappa$ is the increment of $\kappa$ in the time interval $\Delta t$.

Equation (5a) is valid only for loading states ($\Delta\kappa > 0$). If $\Delta\kappa < 0$ after $\kappa > \kappa_e$, elastic unloading or reversed yielding will take place and the $M$-$\kappa$ relation follows the curve ABC shown in Fig. 2, which is based on the elastic-perfectly plastic property of the material. Thus, in the case of unloading and reversed yielding, i.e. for $\Delta\kappa < 0$, the moment-curvature relationship is given by

$$M = \begin{cases} M^* - EI(\kappa^* - \kappa), & \kappa^* - 2\kappa_e \leqslant \kappa \leqslant \kappa^*; \\ M_e\left[-\dfrac{3}{2} - \dfrac{1}{2}\left(\dfrac{\kappa_e}{\kappa^*}\right)^2 + 4\left(\dfrac{\kappa_e}{\kappa^* - \kappa}\right)^2\right], & -\kappa^* \leqslant \kappa \leqslant \kappa^* - 2\kappa_e; \\ M_e\left[-\dfrac{3}{2} - \dfrac{1}{2}\left(\dfrac{\kappa_e}{\kappa}\right)^2\right], & \kappa \leqslant -\kappa^*, \end{cases} \tag{5b}$$

where $\kappa^*(>\kappa_e)$ and $M^*$ $(>M_e)$ are the curvature and bending moment, respectively, of the cross-section at the instant when unloading starts.

### 2.3. *Governing equations and discretization*

The equation of motion, eqn (4), together with the constitutive eqn (5) forms a closed set of non-linear partial differential equations with floating boundaries between various regions, e.g. between elastic and plastic regions, and plastic loading and unloading regions. It is difficult, if not impossible, to obtain an analytical solution for this floating boundary-value problem in a finite beam. Therefore, numerical techniques are applied which are more convenient and capable of predicting the entire dynamic response of a beam from the early wave motion to the final deformation.

Equations (4) and (5) can be rewritten in finite difference form. In the case of projectile impact, we assume that the projectile adheres to the beam during the dynamic response of the beam and no shearing takes place due to impact. If the beam is divided into elements of length $\Delta x_i$, then for an element at the $i$th position, and the equations of motion when $p = 0$ are recast as

$$\begin{aligned} J\ddot{w}_{i+1} - [2J + m(\Delta x_i)^2]\ddot{w}_i + J\ddot{w}_{i-1} &= M_{i+1} - 2M_i + M_{i-1}, \quad (i = 2, \ldots, n) \\ J\ddot{w}_2 - [J + G\Delta x_1 + m(\Delta x_1)^2]\ddot{w}_1 &= M_2 - M_1, \quad (i = 1) \end{aligned} \tag{6}$$

where $G$ is one half of the projectile's mass striking at the mid-span of the beam; $J = mh^2/12$ and $m$ are the rotary inertia and the mass, respectively, of the beam per unit length.

The constitutive relation is written as

$$M_i = \begin{cases} EI\kappa_i, & 0 \leqslant \kappa_i \leqslant \kappa_e; \\ M_e\left[\dfrac{3}{2} - \dfrac{1}{2}\left(\dfrac{\kappa_e}{\kappa_i}\right)^2\right], & \kappa_e < \kappa_i, \quad \Delta\kappa_i \geqslant 0, \end{cases} \tag{7a}$$

during loading ($\Delta\kappa_i \geqslant 0$), and

$$M_i = \begin{cases} M_i^* - EI(\kappa_i^* - \kappa_i), & \kappa_i^* - 2\kappa_e \leqslant \kappa_i \leqslant \kappa_i^*; \\ M_e\left[-\frac{3}{2} - \frac{1}{2}\left(\frac{\kappa_e}{\kappa_i^*}\right)^2 + 4\left(\frac{\kappa_e}{\kappa_i^* - \kappa_i}\right)^2\right], & -\kappa_i^* \leqslant \kappa_i \leqslant \kappa_i^* - 2\kappa_e; \\ M_e\left[-\frac{3}{2} - \frac{1}{2}\left(\frac{\kappa_e}{\kappa_i}\right)^2\right], & \kappa_i \leqslant -\kappa_i^* \end{cases} \tag{7b}$$

during unloading and reversed yielding ($\Delta\kappa_i < 0$). In eqn (7b), $\kappa_i^*$ and $M_i^*$ denote the curvature and bending moment, respectively, of the element at the $i$th position at the instant when unloading starts at this element.

In all cases, the curvature of the $i$th element is related to the transverse displacement by

$$\kappa_i = \frac{w_{i+1} - 2w_i + w_{i-1}}{(\Delta x_i)^2},$$

$$\dot{\kappa}_i = \frac{\dot{w}_{i+1} - 2\dot{w}_i + \dot{w}_{i-1}}{(\Delta x_i)^2}. \tag{8}$$

Solving these equations provides the instantaneous values of accelerations $\ddot{w}_i$ at instant $t_j$, thus for the next instant $t_{j+1} = t_j + \Delta t$, the displacement $w_{i,j+1}$ in the finite difference notation is given by

$$w_{i,j+1} = \ddot{w}_{i,j}(\Delta t)^2 + 2w_{i,j} - w_{i,j-1}. \tag{9}$$

Accordingly, at instant $t_{j+1}$, the curvature $\kappa_{i,j+1}$ at the $i$th position is calculated by eqn (8), and $M_{i,j+1}$ is then calculated by making use of eqn (7).

### 2.4. *Computational procedure*

The computational procedure is summarized as comprising the following steps when quantities $w_{i,j}$ and $M_{i,j}$ are known for all the points in the beam at time $t_j$:

(i) solving algebraic linear eqn (6), calculate acceleration $\ddot{w}_{i,j}$ at instant $t_j$;
(ii) using eqn (9), calculate displacement $w_{i,j+1}$ at instant $t_{j+1} = t + \Delta t$;
(iii) using eqns (8) and (7), calculate values of $\kappa_{i,j+1}$ and $M_{i,j+1}$ at instant $t_{j+1}$.

This cycle of computation then continues, step by step, so that all of the quantities in the response process at any time are obtained until the end of the response.

## 3. NUMERICAL RESULTS AND DISCUSSION

### 3.1. *Example 1 : a free-free beam subjected to impact at mid-span*

For a free-free beam subjected to impact at its mid-span, the deformation of the beam is symmetric about the mid-point $x = 0$, refer to Fig. 1(a); thus, only the right half of the beam with $0 \leqslant x \leqslant L$ is considered in the following analysis. The symmetry conditions at $x = 0$ and the boundary conditions at $x = L$ are

$$Q = 0, \quad \mathrm{d}w/\mathrm{d}x = 0, \quad \text{at } x = 0,$$
$$Q = 0, \quad M = 0, \quad \text{at } x = L. \tag{10}$$

The parameters selected for one half of a free-free beam in this example are similar to those used in work by Symonds (1953) and Symonds and Fleming (1984) for a cantilever beam, namely:

| | |
|---|---|
| half-length of beam | $L = 355.6$ mm; |
| width of beam | $b = 16.3$ mm; |
| depth of beam | $h = 4.5$ mm; |
| mass per unit length of beam | $m = 0.5758$ kg/m; |
| rotary inertia per unit length of beam | $J = 0.972 \times 10^{-6}$ kg m; |

| | |
|---|---|
| half of impact mass | $G = 0.336$ kg; |
| initial velocity of impact mass | $V_0 = 12.9$ m/s; |
| Young's modulus | $E = 206.9$ GN/m$^2$; |
| yield stress | $Y = 200.0$ MN/m$^2$; |
| fully plastic bending moment | $M_p = 16.5$ Nm; |

number of elements in one half of the beam = 28, i.e. $\Delta x = 12.7$ mm.

*The transient behaviour of the beam.* The bending moment diagrams along the right half of the beam at various instants during the response are plotted in Fig. 3(a–d), from which the early response of the beam can be divided into four phases.

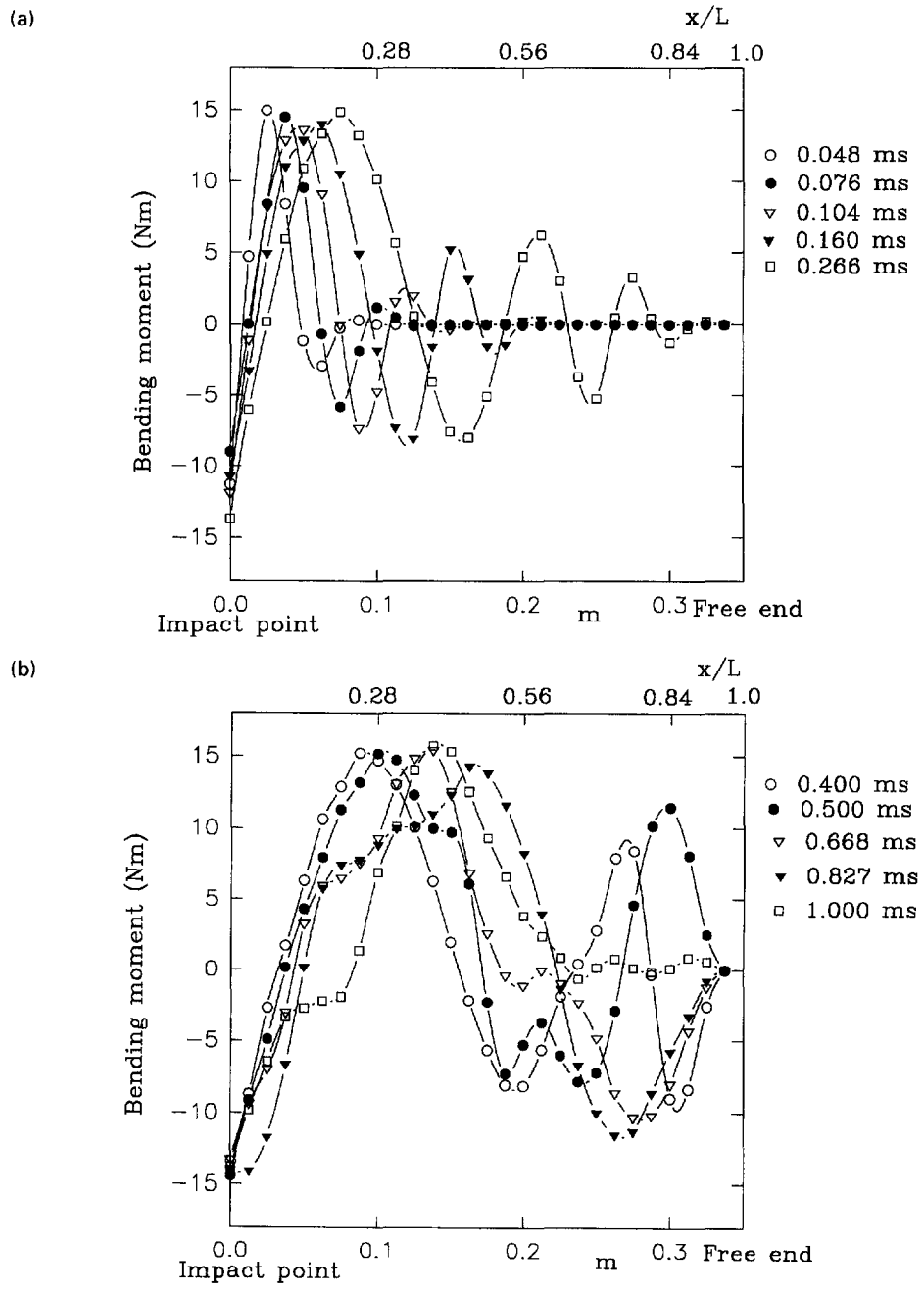


Fig. 3. Bending moment diagrams at various instants, showing flexural wave motion. (*Continued overleaf.*)

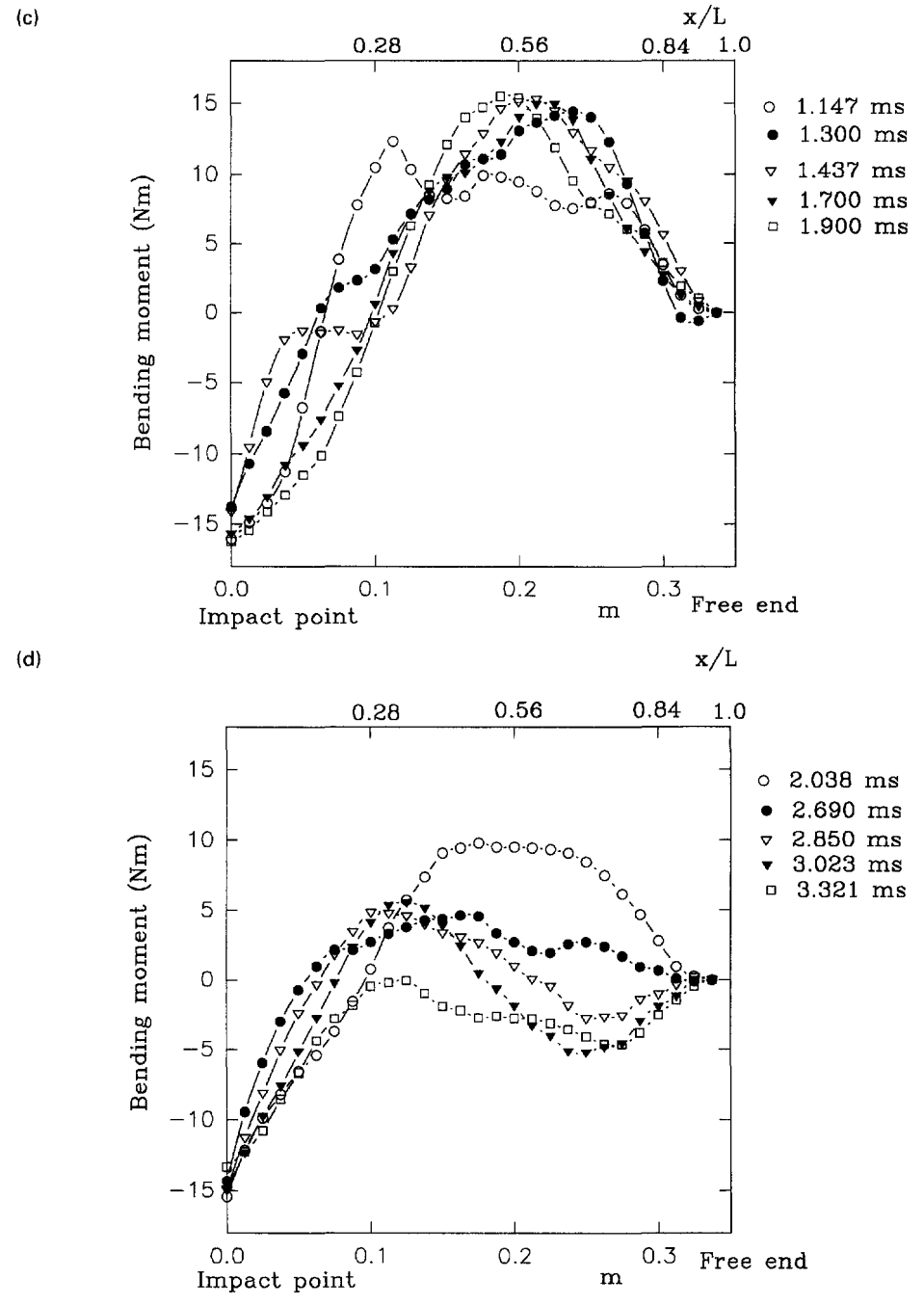


Fig. 3. *Continued.*

Phase 1. Elastic-plastic flexural wave (Fig. 3(a)). Immediately after impact, the effect of the propagation of the flexural wave is similar to that described by Reid and Gui (1987) for a cantilever beam at an early stage. The moment diagram is oscillatory in nature and the dispersion of the flexural wave is evident in the increase in the number of oscillations in the wave packet as the higher frequency components move out ahead of the main disturbance. There is a maximum bending moment close to $M_p$ at instant $t = 0.266$ ms. Compared with the rigid-plastic analysis in the transient phase, the propagation of the maximum bending moment reported here corresponds to the travelling hinge, while the reverse maximum bending moment at the mid-span corresponds to a stationary hinge. For convenience, the terms "travelling hinge" and "stationary hinge" will be used in the following for these features.

Phase 2. First appearance of moving back and forth of the travelling hinge (Fig. 3(b)). The front of the elastic flexural wave reflects at the free end, propagates in the direction opposite to the travelling hinge, and then encounters it at a certain time. The interference between the two waves leads to a re-distribution of the bending moment along the beam. The travelling hinge may retain its maximum bending moment at a magnitude close to $M_p$ or suffer a degree of unloading. This depends upon the difference in the phases of the reflected elastic wave and the front of the plastic wave at the point of encounter. Consequently, the travelling hinge presents a feature that looks as if it moves back and forth. This happens in the time interval from 0.6 to 1.0 ms, and the hinge position is about 0.15 m (about 2/5 of the half length) away from the mid-span. This is different from the case of a cantilever beam (see Reid and Gui (1987)) in which the position is about half the length of the beam.

Phase 3. Second appearance of moving back and forth of travelling hinge (Fig. 3(c)). Over the time interval from 1.0 ms to 1.15 ms, the maximum bending moment is small in magnitude compared with the full plastic bending moment, whilst the travelling hinge seems to vanish as evident in Fig. 3(c). It reappears when the bending moment rises to $M_p$ again at 1.437 ms. As the free-free beam requires the bending moment to be zero at $x = L$, the travelling hinge can never reach the free end of the beam. It is found that the travelling hinge again moves back and forth until $t = 1.9$ ms. The position is around 0.23 m ($\approx 0.65L$) away from the mid-span.

Phase 4. Rotation about the stationary static plastic hinge at the mid-span (Fig. 3(d)). Approximately starting from 2.0 ms, the travelling hinge completely vanishes and only a negative stationary hinge at the mid-span exists in the beam as shown in Fig. 3(d). The two halves of the beam rotate with respect to each other about this hinge at the mid-span. This corresponds to the modal phase in the rigid-plastic analysis; but in elastic-plastic analysis, the reverse stationary hinge undergoes an expanding-and-shrinking period from 4.9 ms to 6.0 ms. As a result, a negative curvature is formed in the neighbourhood of the mid-span. Finally, when the plastic dissipation is complete at the stationary hinge, the whole beam continues to move as a rigid body and a residual elastic vibration remains.

It should be noted that the mass centre of the beam always retains its uniform velocity, $V_c$, in all the phases described above. From the conservation of momentum it is found that

$$V_c = V_o G/(G+mL). \tag{12}$$

Consequently, the kinetic energy of rigid-body motion, i.e. the kinetic energy carried by the mass centre of the beam and the projectile, is given by

$$K_c = \tfrac{1}{2}(G+mL)V_c^2 = \frac{1}{2}\cdot\frac{G^2}{G+mL}V_o^2, \tag{13}$$

which is obviously a constant for this example.

*Distribution of curvature.* The instantaneous distributions of curvature in the beam are depicted in Fig. 4. The mid-span takes the highest value of curvature in the entire response process. Related to phases 2 and 3 described in the previous section, two other peak values of curvature in the interior of the beam appear (at $x = 0.4L$ and $x = 0.65L$), predicted by the present elastic-plastic model.

The final distribution of the curvature based on a rigid, perfectly-plastic model (see Appendix I) and that based on the present elastic-plastic model are both shown in Fig. 4. It should be noted that the final distributions of curvature in the beam (especially in the middle segment, say, $x < 0.2L$) predicted by these two models have very different features. The rigid-plastic model predicts positive curvature along the whole beam with no peak appearing in the interior of the beam, except at the mid-span which is a singular point at which an infinite negative curvature occurs. The discontinuous change from the negative infinite curvature to a positive one at the mid-span is attributed to the discontinuity of the initial velocity distribution at the mid-span and the subsequent pair of plastic hinges

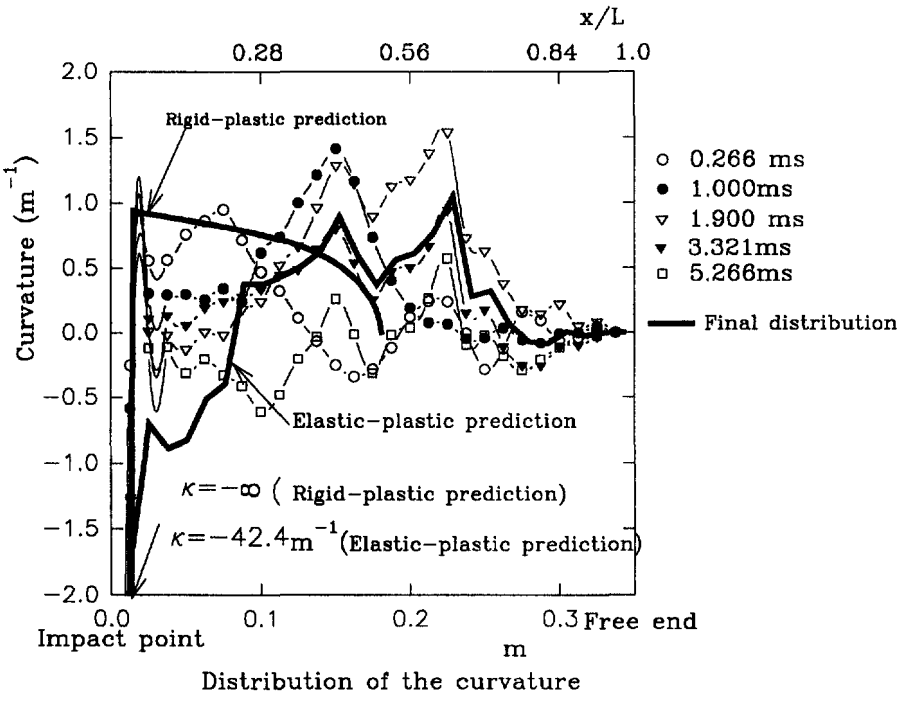


Fig. 4. Evolution of the distribution of curvature.

travelling apart from that point. (If a force of finite magnitude is applied instead of a suddenly imposed velocity at the mid-span, rigid segments of zero curvature will appear which separate the regions of positive curvature from the mid-span, see Lee and Symonds (1952).) In contrast, the elastic-plastic model predicts a region of negative curvature in the middle segment which includes the mid-span where $\kappa = -42.1\ \mathrm{m}^{-1}$. This finite length region of negative curvature is present in the experimental observations as will be seen in Section 5.

*Terminal position of the travelling hinge.* In the rigid-plastic analysis of a free-free beam subjected to impact at its mid-span, the deformation mechanism of the beam in the transient stage consists of a stationary plastic hinge at the mid-span and two travelling hinges moving away from it, see Appendix I. When the travelling hinges cease to move and vanish, the transient stage ends and then each half of the beam rotates about the stationary hinge as a rigid body. The terminal position of the travelling hinge, $\Lambda$, is found to satisfy a cubic equation as (see Appendix 1 for the derivation):

$$\lambda^3 - 4\lambda^2 - 2(4\beta - 1)\lambda + 4\beta = 0, \tag{14}$$

where $\lambda = \Lambda/L$ and $\beta = G/mL$. Hence, in particular,

(i) $\Lambda = 0.586L$, when $\beta \to 0$ (for light mass impact);
(ii) $\Lambda = 0.50L$, when $\beta \to \infty$ (for heavy mass impact), and
(iii) $\Lambda = 0.508L$, when $\beta = 1.64$ (for example 1 in the present paper).

It is evident that for any value of $\beta = G/mL$ the terminal position of the travelling hinge lies between $0.5L$ and $0.586L$ according to the rigid-plastic theory. For the elastic-plastic analysis presented here, the travelling hinge vanishes at the end of phase 2. Estimated from Fig. 5, the terminal position is about $0.61L$ while the experimental data gives approximately $0.62L$ for $G/mL = 6$. According to the calculation based on the elastic-plastic analysis, the terminal position of the travelling hinge is insensitive to the mass ratio $G/mL$. This is in accord with that based on the rigid-plastic analysis.

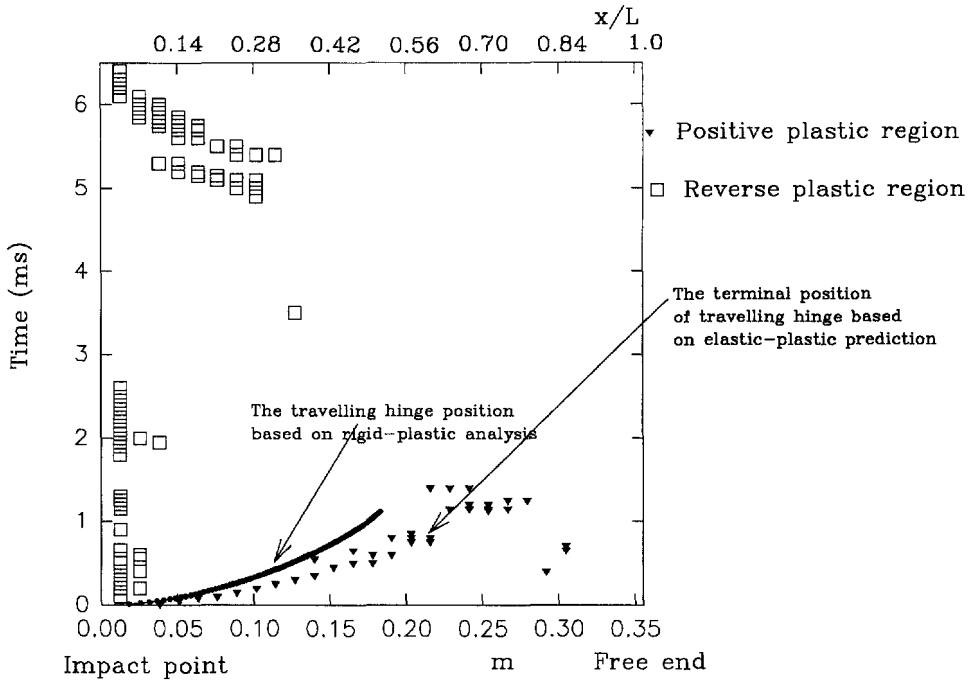


Fig. 5. Evolution of the plastic region in a beam subjected to impact at its mid-span.

*Instantaneous profiles of beam.* Figures 6(a) and (b) depict the instantaneous profiles of the deformed beam obtained from the elastic-plastic analysis and rigid-plastic analysis. The time instants are selected so as to correspond to the end of each phase. The instantaneous flying shapes of the beam based on the elastic-plastic prediction agree well with those obtained by high-speed photography as described in Section 5 below. The rigid-plastic model gives quite a good prediction of the deflection at the impact point ($x = 0$) in comparison with elastic-plastic analysis.

*Energy partitioning.* In order to obtain a quantitative evaluation of the elastic effect, an energy ratio $R$ is introduced that is defined by

$$R = W_o / W_e^{max}, \tag{15}$$

where $W_o = GV_0^2/2$ is the initial kinetic energy, and $W_e^{max}$ is the maximum elastic deformation energy which can be stored in the beam. The plastic dissipation, $W_p$, is calculated from

$$W_p = \sum_{i=1}^{n} \left( \int_0^t M_i \kappa_i \Delta x_i \, dt - M_i^2(t) \Delta x / 2EI \right), \quad \kappa_i > 0, \tag{16}$$

while the final kinetic energy of the rigid-body motion, $K_c$, is obtained by eqn (13). According to eqn (1), therefore, the elastic deformation energy in the final residual vibration stage is estimated by

$$W_e = W_o - (W_p + K_c). \tag{17}$$

Figure 7 displays how the partitioning of the total input energy varies with the energy ratio $R$ in the case where $G/mL = 1.64$. A large amount (about 62%) of the input energy is converted into the kinetic energy of rigid-body motion. When $R \to \infty$, approximately 38% of the input energy is dissipated plastically. If $R = 2$, however, the portion reduces to 21% and the remaining 17% of the input energy is converted into the elastic deformation energy.

(a)

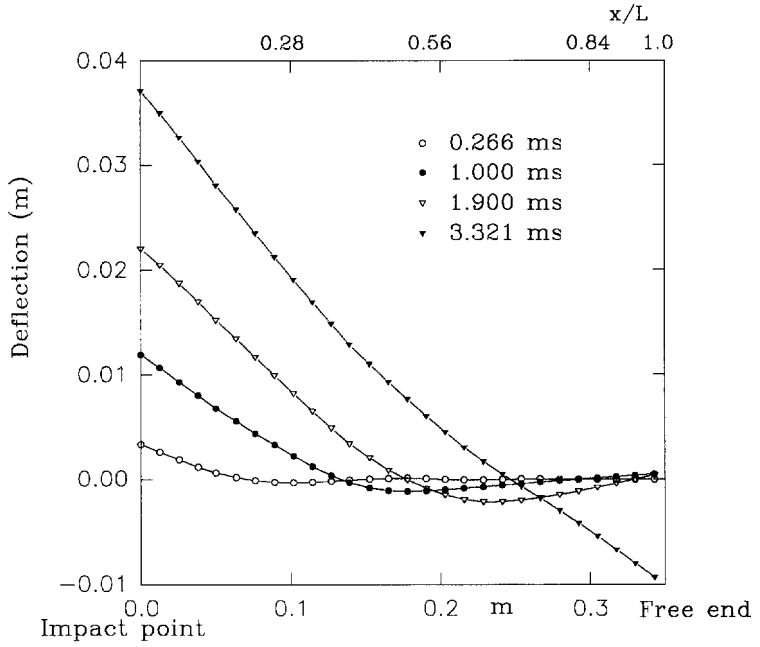


(b)

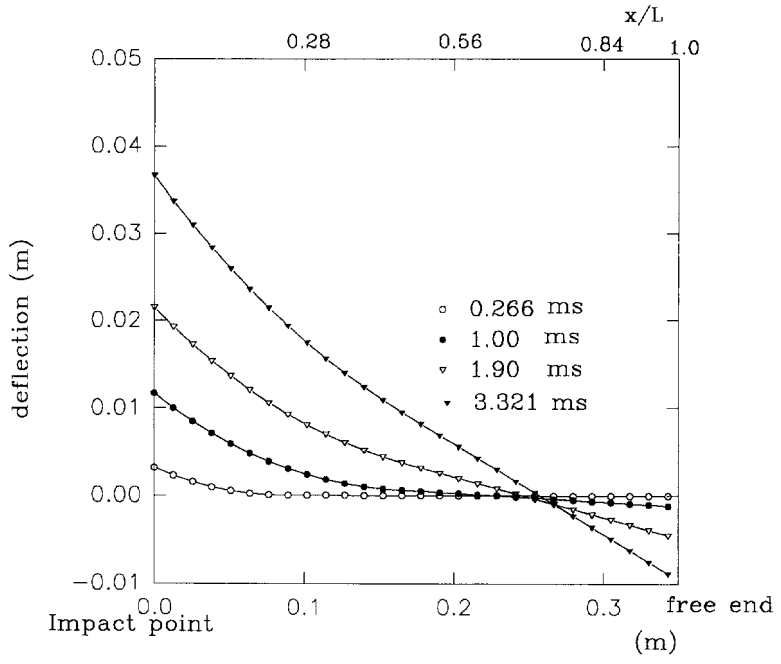


Fig. 6. Instantaneous profiles of a beam subjected to impact at its mid-span, predicted by (a) the elastic-plastic model and (b) the rigid-plastic model.

### 3.2. *Example 2: a free-free beam subjected to a triangular impulsive loading*

When a free-free beam is subjected to a triangular impulsive loading, as shown in Fig. 1(b), the initial flexural wave propagation and subsequent interaction with the plastic front in the transient stage are somewhat similar to those in Example 1. According to the rigid-plastic analysis given by Jones and Wierzbicki (1987), the valid deformation mechanism which provides a complete solution contains only a single-stationary plastic hinge at the mid-span. The present elastic-plastic analysis, however, demonstrates that a plastic front, like a travelling hinge, propagates during the response of the beam. The evolution of the plastic region in the beam for this case is depicted in Fig. 8.

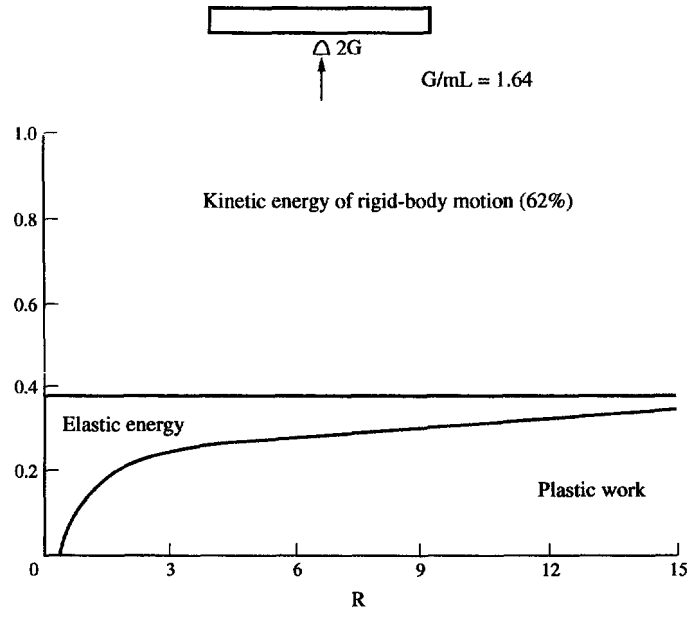


Fig. 7. Energy partitioning for a beam subjected to impact at its mid-span.

Instead of fully discussing the detailed behaviour of the beam in the transient stage, we focus our attention on the partitioning of the input energy, which is given in Fig. 9. The difference between the elastic-plastic and rigid-plastic analyses is attributed to the contribution of the elastic deformation energy that can occupy a fraction of the same order as that of plastic dissipation when $R < 6$ and there is a small regime of $0 < R < 1.25$ in which no plastic dissipation is produced at all.

*Influence of slenderness ratio* L/h. In order to understand the influence of the ratio of the length to the depth of the beam on the energy partitioning, another case in which the

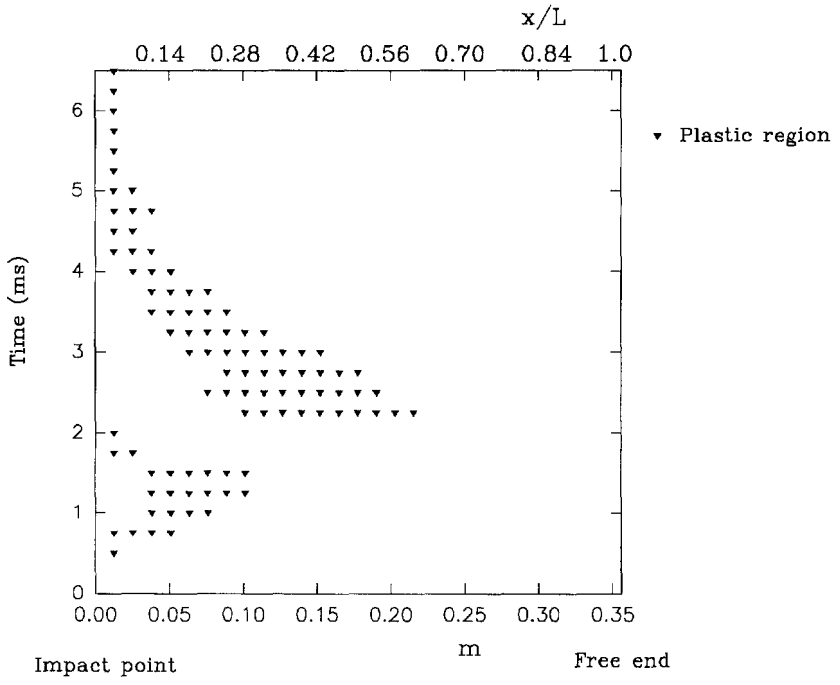


Fig. 8. Evolution of the plastic region in a beam subjected to triangularly distributed impulsive loading.

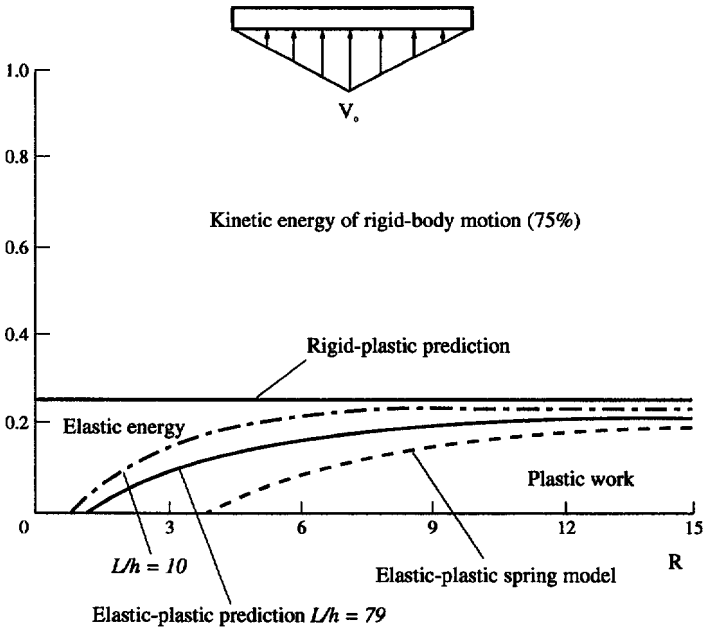


Fig. 9. Energy partitioning for a beam subjected to triangularly distributed impulsive loading.

response of a beam of half length, $L$, equal to 45 mm (slenderness ratio $L/h = 10$) under otherwise identical conditions is calculated. The result, which is depicted as the chain line in Fig. 9, indicates that the portion of the plastic dissipation is larger than that of the previous case of $L/h = 79$ ($h = 4.5$ mm) for the same value of $R$. On the other hand, since the kinetic energy of final rigid-body motion remains a constant fraction of 75% of the input energy regardless of the slenderness ratio of the beam, in the case of smaller slenderness ratios the elastic deformation energy occupies a smaller proportion. For the example of $L/h = 10$, according to Fig. 9, the elastic deformation energy is less than 5% of the input energy when $R > 6$. This indicates that the rigid-plastic theory provides a better approximation for short beams than for slender beams.

*The "error" of the rigid-plastic model.* Further comparison between the elastic-plastic and rigid-plastic model can be performed by introducing two parameters, viz. $(W_p^r - W_p^e)/W_p^e$ and $W_p^e/W_e^{max}$ where $W_p^r$ denotes the plastic work resulting from the rigid-plastic model and $W_p^e = W_p$ defined in eqn (16) is obtained from the elastic-plastic analysis and is regarded as the "actual" value. Hence, parameter $(W_p^r - W_p^e)/W_p^e$ represents the "error" introduced by making the rigid-plastic idealization. On the other hand, the ratio of the plastic dissipation to the maximum elastic deformation energy which can be stored in the beam, $W_p^e/W_e^{max}$, serves as an index of the relative insignificance of elasticity in the problem. Figure 10 depicts the correlation between these two parameters (the "error" of the rigid-plastic analysis and the energy index) for a free-free beam subjected to impact at the mid-span or to a triangular loading. It is shown that with the increase of $W_p^e/W_e^{max}$, the relative discrepancies between $W_p^e$ and $W_p^r$ tend to zero, which implies that the neglect of elasticity become more reasonable. When $W_p^e/W_e^{max}$ is less than 2, however, the error caused by the rigid-plastic model becomes so large that ignoring elastic effect is unacceptable.

## 4. A SIMPLIFIED ELASTIC-PLASTIC MODEL

In order to further understand the contribution of the elastic effect, a simple structural model is constructed. The model consists of two halves of a rigid, perfectly-plastic free beam connected by an elastic-plastic rotational spring at the mid-span. This kind of model was previously studied by Wang and Yu (1991) for the dynamic behaviour of a cantilever beam. Similar to Example 2 illustrated above, assume that at the initial instant, a triangular

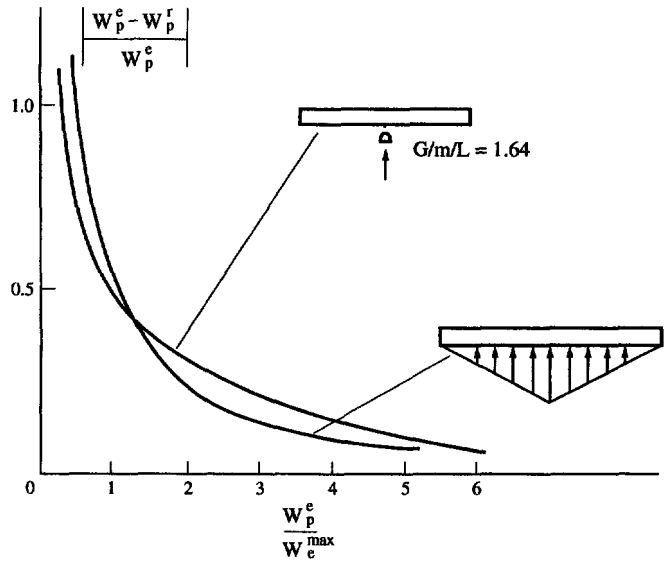


Fig. 10. The "error" of the rigid-plastic model in the plastic dissipation compared with the elastic-plastic model.

impulsive loading is applied and results in a triangular initial velocity distribution along the beam, as shown in Fig. 11. The behaviour of the spring is assumed to be described by

$$M_s = \begin{cases} k(\theta - \theta_p), & \text{elastic or unloading;} \\ M_e \text{ or } -M_e, & \text{otherwise,} \end{cases} \tag{18}$$

where $k$ is the elastic constant, $\theta_p$ is the plastic rotation angle, and $M_e$ is the maximum elastic bending moment of the beam. The elastic constant, $k$, of the spring can be approximately determined by an energy equivalence. For a beam with flexural rigidity $EI$ and length $L$, the maximum elastic deformation energy which can be stored in the beam is $W_e^{max} = M_e^2 L/2EI$, while the maximum elastic deformation energy of the spring is $M_e^2/2k$. The equivalence of these two gives

$$k = EI/L. \tag{19}$$

More details of the formulation of the model are given in Appendix II. The various portions of the energy are

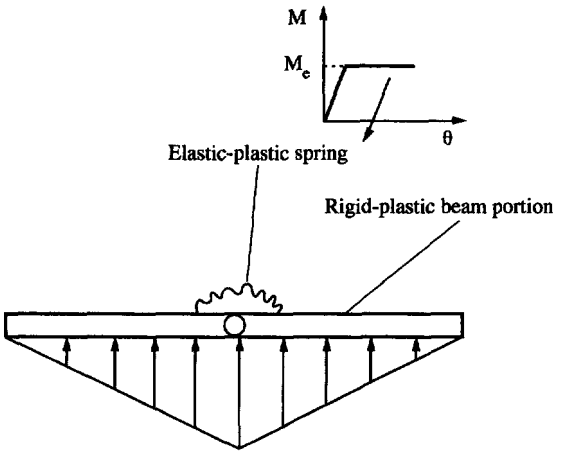


Fig. 11. A simplified beam-spring model.

$$W_o = mLV_o^2/6, \quad K_c = mLV_o^2/8, \quad W_p = mLV_o^2/24 - M_c^2 L/2EI, \quad W_e = M_e^2 L/2EI. \tag{20}$$

The energy ratio $R$ is defined by eqn (15) as before.

The ratios of various portions of energy to total input energy are also shown in Fig. 9, in which the dashed line represents the boundary between the elastic and plastic portions of the energy based on the beam-spring model. There is a minimum value of $R = 4$, below which no plastic dissipation occurs in the beam; in other words, when $R \leqslant 4$, the total input energy is only converted into kinetic energy of rigid-body motion and the elastic deformation energy. This obviously underestimates the contribution of the plastic dissipation to the deformed beam. On the other hand, the rigid-plastic analysis given by Jones and Wierzbicki (1987) evidently overestimates the contribution of the plastic dissipation, which is also shown in Fig. 9.

## 5. COMPARISON WITH EXPERIMENTS

The theoretically predicted behaviour of a free-free beam subjected to impact by a projectile at the mid-span, based on the elastic-plastic analysis, can be compared with results obtained from high-speed photographs of experiments conducted by one of the authors (CDA). In one of these tests a free-free mild steel beam was struck by a sledge of mass ($2G = 525$ g), which was large compared with the mass of the beam ($\beta = G/mL = 6$), travelling at an initial speed of 15 m/s. The annealed mild steel beam had a rectangular cross-section; its thickness, width and length were 3.18 mm, 12.7 mm and 279.4 mm, respectively. The stress-strain curve for the material of the beam is given in Fig. 12(a) and the measured values for yield stress, Young's modulus and strain hardening modulus were $Y = 207.5$ MN/m$^2$, $E = 199.0$ GN/m$^2$ and $E_p = 570$ MN/m$^2$, respectively.

The test was photographed using a high speed Imacon camera operating at a fixed framing rate of 10,000 f/s. The aim was to examine the kinematics of the deformation of the beam and gain some insight into the instantaneous profiles of the beam in the transient phase.

In the corresponding calculation, all parameters of the load and the beam are chosen the same as those in the test, while the stress-strain curve of the real material shown in Fig.

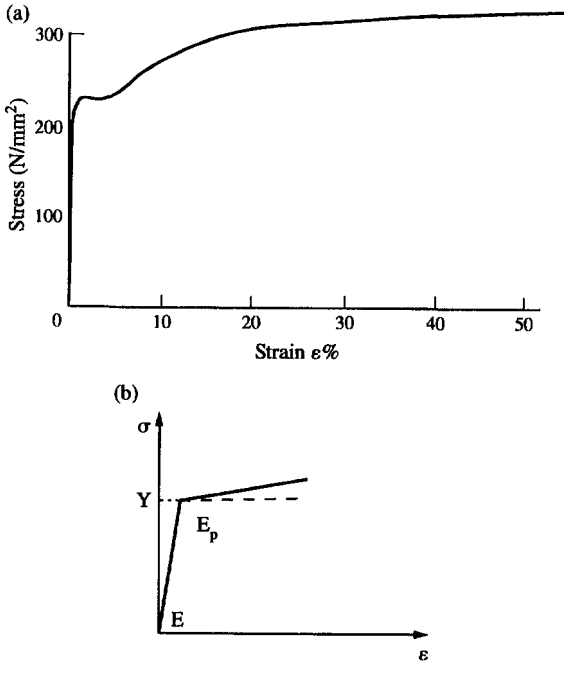


Fig. 12. The stress-strain relation for annealed mild-steel specimens: (a) the experimental curve; (b) a bi-linear model.

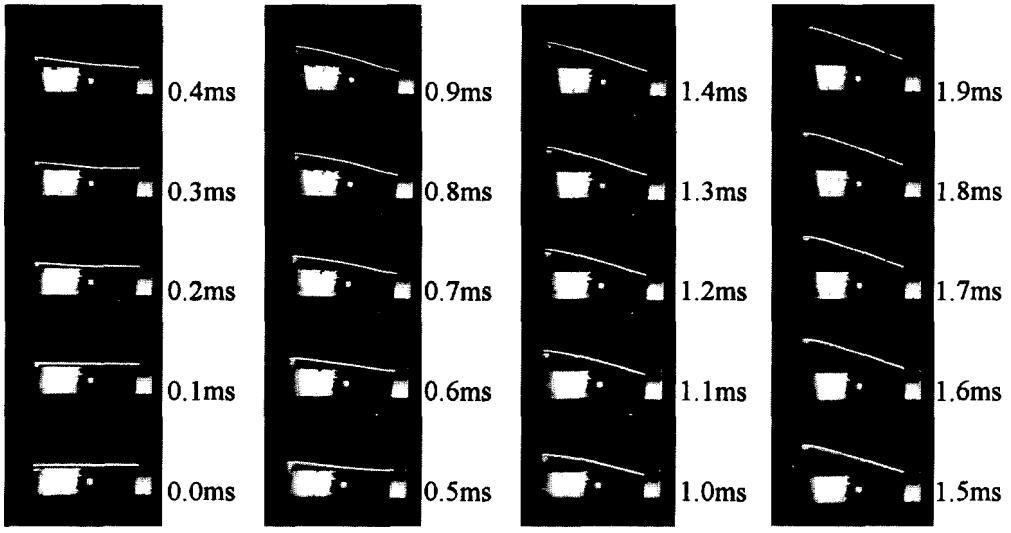


Fig. 14. A group of high-speed photographs of a mild steel beam struck by a projectile of mass 525 g travelling at 15 m/s. Triggering the Imacon camera at different times before and after the impact enables a complete picture of the deformation process to be assembled.

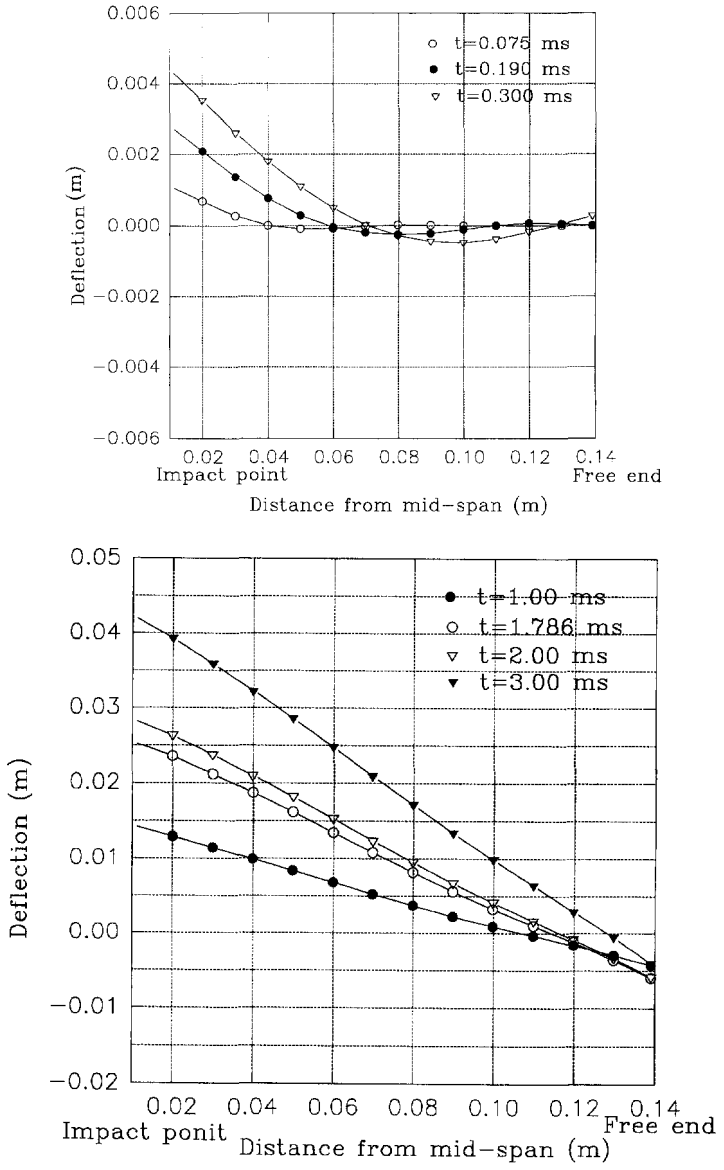


Fig. 13. Instantaneous profiles of the beam predicted by the elastic-plastic model.

12(a) is approximated by a bi-linear relation shown in Fig. 12(b), with $Y$, $E$, and $E_p$ being specified above. The theoretical predictions of the instantaneous profiles of the free-free beam due to an initial velocity 15 m/s are plotted in Fig. 13(a) and (b). As a comparison, a set of high-speed photographs taken from a series of tests on such beams is reproduced in Fig. 14. By comparing typical instantaneous profiles (e.g. those at $t = 0.1$ ms and 0.3 ms, i.e. for early times and the simpler modes at later times) shown in Figs 13 and 14, it can be seen that the present theoretical predictions of the instantaneous profiles have captured the main features of the experimental observations.

## 6. CONCLUSIONS

(1) The dynamic behaviour of a free-free beam subjected to impact by a projectile at the mid-span or to triangular impulsive loading has been studied based on an elastic-plastic constitutive relation and a relevant numerical procedure. The numerical results when compared with the instant profiles experimentally obtained from high-speed photographs, show good agreement.

(2) The interference between the plastic flexural wave and the elastic flexural wave reflected at the free-end plays a major role in determining the deformed profile of a free-free beam under intense dynamic loading. As the plastic dissipation mainly appears in the early phases of the response, the final irreversible deformation of a free-free beam is dominated by that gained in the transient stage.

(3) The total input energy (or the work done by the external load) to the beam is converted into three portions, i.e. the kinetic energy of rigid-body motion, the plastic dissipation and the elastic deformation energy. The rigid, perfectly-plastic approach overestimates the contribution of the plastic dissipation in the beam, while a simple beam-spring model tends to underestimate this contribution. This overestimate/underestimate may lead to an incorrect prediction of plastic collapse of the structure. Especially, in the case of relatively small $R$, only an elastic-plastic analysis such as that presented in this paper can provide a more precise prediction on the plastic dissipation and the possible failure of the dynamically loaded free-free beams.

## REFERENCES

Hall, R. G., Al-Hassani, S. T. S. and Johnson, W. (1971). The impulsive loading of cantilever. *Int. J. Mech. Sci.* **13,** 415–430.

Jones, N. and Wierzbicki, T. (1987). Dynamic plastic failure of a free-free beam. *Int. J. Impact Engng* **6,** 255–240.

Lee, E. H. and Symonds, P. S. (1952). Large plastic deformations of beam under transverse impact. *J. Appl. Mech.* **19,** 308–314.

Reid, S. R. and Gui, X. G. (1987). On the elastic-plastic deformation of cantilever beams subjected to tip impact. *Int. J. Impact Engng* **6,** 109–127.

Symonds, P. S. (1953). Dynamic load characteristics in plastic bending of beams. *J. Appl. Mech.* **20,** 475–481.

Symonds, P. S. and Fleming, W. T., Jr (1984). Parkes revisited: on rigid-plastic and elastic-plastic dynamic structural analysis. *Int. J. Impact Engng* **2,** 1–36.

Symonds, P. S. and Leth, C. F. A. (1954). Impact of finite beam of ductile metal. *J. Mech. Phys. Solids* **2,** 92–102.

Wang, X. D. and Yu, T. X. (1991). Parkes revisited: effect of elastic deformation at the root of a cantilever beam. *Int. J. Impact Engng* **11,** 127–209.

## APPENDIX I

*Rigid-plastic analysis for a free-free beam subjected to impact by a travelling mass at the mid-span cross-section*

When a rigid-plastic free-free beam is subjected to transverse impact at its mid-point by a rigid mass $2G$ moving at initial speed $V_0$, the response of the beam consists of two phases. In the first phase, $0 \leqslant t \leqslant t_1$, a stationary plastic hinge forms at the impact point (i.e. the mid-point of the beam), and two travelling plastic hinges move outwards from that point until their travelling velocities become zero. In the second phase, $t_1 < t \leqslant t_2$, the stationary hinge still exists while the two travelling hinges vanish and each half of the beam rotates about the stationary hinge as a rigid-body until the angular velocity is equal to zero.

Phase 1: $0 \leqslant t \leqslant t_1$. Figure A.1 shows the velocity diagram of the left half of the beam. The travelling hinge $H$ is distance $\Lambda(t)$ away from the stationary hinge $A$. The upward velocity of the point at distance $x_1$ from $A$ in section $AH$ is

$$\dot{y}_1 = \dot{U} - x_1\dot{\theta}, \tag{A1}$$

where $U$ denotes the transverse displacement of the mid-point. The upward velocity of the point at distance $x_2$ from $A$ in section $HB$ is

$$\dot{y}_2 = \dot{U} - \Lambda\dot{\theta} - (x_2 - \Lambda)\dot{\phi}. \tag{A2}$$

Thus, the accelerations of these two points are

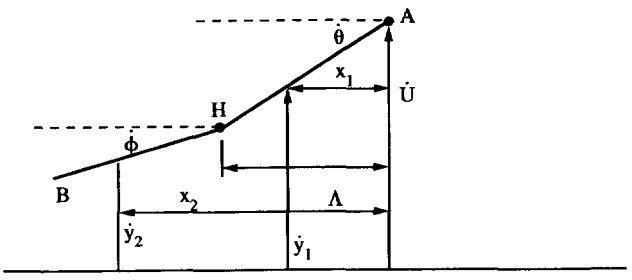


Fig. A1. Velocity diagram in phase 1.

$$\ddot{y}_1 = \ddot{U} - x_1\ddot{\theta},$$
$$\ddot{y}_2 = \ddot{U} - \Lambda\ddot{\theta} - (x_2 - \Lambda)\ddot{\phi} + \Lambda\phi - \Lambda\dot{\theta}. \tag{A3}$$

By taking the momentum and moment of momentum of sections $AH$ and $HB$, the governing equations are found to be

$$-G\ddot{U} = \int_0^{\Lambda} m\ddot{y}_1 \, dx_1$$
$$2M_P = \int_0^{\Lambda} m\ddot{y}_1 \, dx_1$$
$$0 = \int_{\Lambda}^{L} m\ddot{y}_2 \, dx_2$$
$$M_P = -\int_{\Lambda}^{L} \ddot{y}_2 m(x_2 - \Lambda) \, dx_2. \tag{A4}$$

Substitution of (A3) into (A4) gives

$$(G + m\Lambda)\ddot{U} - \frac{m\ddot{\theta}\Lambda^2}{2} = 0,$$
$$2M_P = m\Lambda^2\left(\frac{\ddot{U}}{2} - \frac{\Lambda\ddot{\theta}}{3}\right),$$
$$\ddot{U} + \Lambda(\dot{\phi} - \dot{\theta}) + \Lambda(\ddot{\phi} - \ddot{\theta}) = \frac{\ddot{\phi}(L + \Lambda)}{2},$$
$$M_P = \frac{m\ddot{\phi}(L - \Lambda)^3}{12}. \tag{A5}$$

After introducing the following non-dimensional quantities

$$u = U/L, \quad \lambda = \Lambda/L, \quad \beta = G/mL, \quad (^{\circ}) = \mathrm{d}(\ )/\mathrm{d}\tau, \quad \tau = t(mL^3/M_p)^{-1/2},$$

eqns (A5) can be rewritten in their non-dimensional forms as

$$\lambda^2\left(\frac{\ddot{u}}{2} - \frac{\lambda\ddot{\theta}}{3}\right) = 2,$$
$$\ddot{u}(\lambda + \beta) - \frac{\ddot{\theta}\lambda^2}{2} = 0,$$
$$\ddot{u} + \dot{\lambda}(\dot{\phi} - \dot{\theta}) + \lambda(\ddot{\phi} - \ddot{\theta}) = \ddot{\phi}\left(\frac{1 + \lambda}{2}\right),$$
$$\frac{\ddot{\phi}(1 - \lambda)^3}{12} = 1, \tag{A6}$$

and it follows that

$$\ddot{u} = \frac{-12}{\lambda(\lambda + 4\beta)}, \tag{A7}$$
$$\ddot{\theta} = \frac{-24(\lambda + \beta)}{\lambda^3(\lambda + 4\beta)}, \tag{A8}$$
$$\ddot{\phi} = \frac{12}{(1 - \lambda)^3}. \tag{A9}$$

The terminal position of the travelling hinge is determined by putting $\dot{\lambda} = 0$ (or $\dot{\phi} - \dot{\theta} = 0$), and note that $u$, $\ddot{\theta}$ and $\ddot{\phi}$ are expressed in terms of $\lambda$. Substituting eqns (A7)–(A9) into the third equation of (A6) leads to

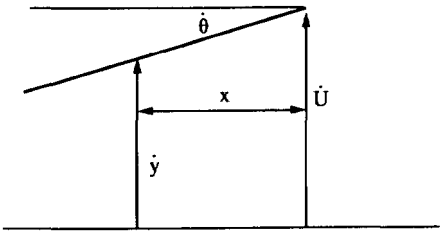


Fig. A2. Velocity diagram in phase 2.

$$\lambda^3 - 4\lambda^2 - 2(4\beta - 1)\lambda + 4\beta = 0. \tag{A10}$$

Phase 2: $t_1 < t \leqslant t_2$. The velocity diagram is as shown in Fig. A2. A point in the beam at distance $x$ away from stationary hinge $A$ has the velocity

$$\dot{y} = \dot{U} - x\dot{\theta}. \tag{A11}$$

Making use of the momentum and moment of momentum equations for segment $BH$, the non-dimensional governing equations are found to be

$$\ddot{u} = \frac{-6}{1+4\beta}$$

$$\ddot{\theta} = \frac{-12(1+\beta)}{1+4\beta}. \tag{A12}$$

The solutions are given by

$$u = u_1 + \dot{u}_1(\tau - \tau_1) - \frac{3}{1+4\beta}(\tau - \tau_1)^2$$

$$\theta = \theta_1 + \dot{\theta}_1(\tau - \tau_1) - \frac{6(1+\beta)}{1+4\beta}(\tau - \tau_1)^2 \tag{A13}$$

in which subscript 1 pertains to the value at the end of phase 1.

## APPENDIX II

*Energy partitioning of a simplified beam-spring model*

Refering to Fig. 11, consider the left half of the beam. When the beam is subjected to a triangular impulsive loading with maximum velocity $V_o$ at the mid-point (see Fig. 1(b)), the initial momentum and input energy are

$$S_0 = \int_0^L \frac{V_0 x m}{L}\,\mathrm{d}x = \frac{mLV_0}{2} \tag{A14}$$

$$W_0 = \int_0^L \frac{1}{2}\left(\frac{xV_0}{L}\right)^2 m\,\mathrm{d}x = \frac{mV_0^2 L}{6}, \tag{A15}$$

respectively. The velocity of the mass centre of the beam is constant and can be obtained by the conservation of momentum. Thus,

$$V_c = V_o/2. \tag{A16}$$

Hence, the kinetic energy of the rigid body motion is

$$K_c = mLV_o^2/8, \tag{A17}$$

and the maximum elastic deformation energy for the beam-spring model is

$$W_e = M_e^2 L/2EI. \tag{A18}$$

According to the conservation of energy, the plastic dissipation is found to be

$$W_p = mLV_o^2/24 - M_e^2 L/2EI. \tag{A19}$$